Research Article

The Study of MgO and/or ZrO_2 Modified Al_2O_3 for CO_2 Adsorption

Thaninee Chandarin, Supachai Jadsadajerm, Tanakorn Ratana, Sabaithip Tungkamani and Monrudee Phongaksorn*
Department of Industrial Chemistry, Faculty of Applied Science, King Mongkut's University of Technology of North Bangkok, Bangkok, Thailand

* Corresponding author. E-mail: monrudee.p@sci.kmutnb.ac.th DOI: 10.14416/j.asep.2022.09.004
Received: 28 April 2022; Revised: 4 June 2022; Accepted: 25 July 2022; Published online: 13 September 2022

Abstract
Alumina (Al_2O_3) is widely used as a sorbent in CO_2 adsorption and as a catalyst support in CO_2 utilization. For this application, the CO_2 adsorption ability is the most important property to be improved. Thus, this work presents the idea to modify the surface of a commercial alumina using an Mg-Zr mixed oxide. With this material, sites for CO_2 adsorption can be created by generating oxygen mobility property simultaneously with the basicity. To prove this hypothesis, alumina modified with MgO, ZrO_2, or Mg-Zr mixed oxide was prepared by an incipient wetness impregnation. The physicochemical properties of the bare alumina and the alumina modified with MgO, ZrO_2, or Mg-Zr mixed oxide were investigated using N_2 adsorption-desorption and X-ray diffraction. The achievement of oxygen mobility creation was quantitatively evaluated by O_2-temperature programmed desorption measurement. The CO_2 adsorption performance with the distribution of basic site strength was determined by CO_2-temperature programmed desorption measurements. According to the results, the highest oxygen mobility was found in the alumina modified with Mg-Zr mixed oxide, which is approximately 1.7 times that of the bare alumina. The alumina modified with Mg-Zr mixed oxide showed the highest CO_2 capacity by approximately 1.4 times compared to the alumina. It is because the cubic ZrO_2 stabilized with MgO provided the number of oxygen vacancy sites that can be filled by oxygen atoms in adsorbed CO_2 corresponding to the moderate and strong basic sites.

Keywords: Oxygen mobility, Solid adsorbent, Alumina, Carbon dioxide capture, Magnesium oxide, Zirconia

1 Introduction

At present, the world is facing a climate crisis due to the rising impact of global warming caused by an increase in the emission of greenhouse gases (Green House Gases (GHG)). Among many greenhouse gases, carbon dioxide (CO_2) emission is considered a major problem because of the CO_2 accumulation in the Earth's atmosphere. In 2021, global CO_2 concentration reaches 415 ppm, 1.5-fold of the CO_2 concentration in 1750 [1]. This concentration is much higher than the safe concentration of CO_2 in the atmosphere (350 ppm) defined by the World Health Organization (WHO) [2]. In order not to release excess CO_2 into the atmosphere, there have been many researches attempts to develop technologies for this purpose.

Renewable energy technologies are considered the clean energy production derived from renewable sources such as biomass, wind, solar, and water. Their availability is still lower than the overall energy demand [3]. CO_2 capture utilization and storage (CCUS) is an essential emissions reduction technique that solves the problem of global warming by reducing CO_2 emissions [4]. CO_2 capture and storage is a set of technologies that capture CO_2 and then inject it into suitable underground storage reservoirs to prevent it from being released into the atmosphere. Rather than being stored underground, many studies utilized the captured CO_2 as a raw material for high value-added products. Thus, various approaches for CO_2 capture have been developed recently, including membrane separation, amine-based solvents, ionic liquids, and

cryogenic fractionation. However, these technologies have the problem of intensive regenerated energy consumption, and environmental corrosion problems [5]. Moreover, the difficulty of CO_2 separation from liquid absorbents is an obstacle to CO_2 utilization. To avoid this problem, the solid adsorbent for CO_2 capture is considered a more appropriate technique due to the easier and lower-cost separation [6].

Solid adsorbents are one of the most environmentally friendly materials involved in CO_2 capture and utilization technique due to their recoverability and reusability [7], [8]. The adsorbents, also known as solid sorbents, require various properties for adsorbing CO_2 consisting of a high specific surface area, pore structure, thermal stability, and basic surface. Adsorbents such as zeolites, carbon-based materials, metal-organic frameworks, and alkaline earth metal oxides have been studied by many works recently [9]–[11]. However, these adsorbents still showed the drawback of thermal and mechanical stability which obstruct their adsorption-regeneration cycle and commercial application.

Alumina (Al_2O_3) is a versatile material, which has many attractive properties including a large surface area, great thermal and mechanical stability, and acid-base surface properties. Consequently, Al_2O_3 is commonly used as an adsorbent as well as a catalyst support. Considering the acid-basic surface properties which show a strong effect on CO_2 adsorption, sites on the Al_2O_3 surface present a stronger acid than a basic [12]. As a result of the acidic nature of CO_2, pure Al_2O_3 has a low CO_2 adsorption capability.

According to certain works, MgO is a promising material, which has high moderate basicity and adsorption/desorption capacities at medium to high temperatures. However, it has a lower surface area and pore structure than Al_2O_3, resulting in a problem of the loss of pore structure with the high regenerating temperatures [13]. ZrO_2 is also attractive as a metal oxide that has been utilized in a variety of catalytic CO_2 utilization due to its acid-basic surface and oxygen vacancy sites [14]–[16]. The appearance of the oxygen vacancy sites can promote basic sites on the surface [17]. The additions of alkaline metal oxides (Na, K) [18], [19], alkaline earth metal oxides (Ca, Mg) [20], [21], and transition metal oxides (Zr, Ni) [22], [23] raised the CO_2 adsorption capacity of Al_2O_3. Wang *et al.* reported that the Al_2O_3 with 30% of MgO loading showed the higher CO_2 adsorption capacity with the greater thermal and mechanical stability than pure Al_2O_3 [6]. Chavez *et al.* [24] studied the influence of Al_2O_3 content on the Al_2O_3-ZrO_2 composite. The ZrO_2 incorporation into Al_2O_3 resulted in increased surface properties, protected sintering effect, and inhibited the crystallization of the γ- Al_2O_3 phase. Yan *et al.* [25] also studied acid-basic site property on $Mg_2Zr_xAl_{1-x}$ mixed metal oxides catalyst for the synthesis of diethyl carbonate from urea and ethanol. The catalyst is derived from layer double hydroxide that MgO and ZrO_2 disperse homogenously in the Al_2O_3 matrix. The characterization results found that acid-base sites of the catalyst facilitate the reactant adsorption mechanism. Moreover, $Mg_2Zr_xAl_{1-x}$ mixed metal oxide provided the greater basic sites than pure Al_2O_3.

However, there was no work studying on the surface of alumina modified with Mg-Zr mixed oxide for the CO_2 adsorption. The purpose of this work is to develop the CO_2 adsorption of the commercial Al_2O_3 surface with Mg-Zr mixed oxide using the uncomplicated preparation method. This study hypothesizes that MgO and ZrO_2 should have a high potential to enhance the basicity of the Al_2O_3 surface due to the basicity of MgO, the oxygen mobility of ZrO_2, and the great interaction of Mg-Zr-Al oxide. As a result, CO_2 adsorption-activation of Al_2O_3 will be then improved significantly. Moreover, the change of oxygen mobility with the CO_2 adsorption strength on the Mg-Zr mixed oxide modified Al_2O_3 surface is an interesting result to be evaluated. Thus, in this study, the CO_2 adsorption capability of the commercial Al_2O_3 was developed by modifying the surface with the co-functional MgO-ZrO_2 mixed oxide and compared to the single MgO and ZrO_2 oxide. MgO and ZrO_2, as a metal oxide and a mixed metal oxide, were dispersed onto Al_2O_3 via the incipient wetness impregnation method. The textural properties of commercial Al_2O_3, 5 wt%MgO-5 wt%MgO/Al_2O_3, 10 wt%MgO/Al_2O_3, and 10 wt%ZrO_2/Al_2O_3 were investigated using N_2 adsorption-desorption isotherm analysis. For the surface characterization, the crystalline phases were interpreted by X-ray diffraction (XRD). The weight percentage was determined via a scanning electron microscope equipped with energy dispersive X-ray spectrometer (SEM-EDX). The oxygen mobility of all samples was evaluated by O_2-temperature programmed desorption (O_2-TPD). The CO_2 adsorption strength and capability were measured employing

CO_2-temperature programmed desorption (CO_2-TPD). All those properties of the MgO-ZrO_2 mixed oxide modified Al_2O_3 sample were compared with other samples and discussed.

2 Experimental Procedure

2.1 *Material preparation*

Samples of 10 wt%MgO/Al_2O_3, 10 wt%ZrO_2/Al_2O_3, and 5 wt%MgO-5 wt%ZrO_2/Al_2O_3 (coded as 10M/A 10Z/A and 5M5Z/A, respectively) were prepared by incipient wetness impregnation method. Al_2O_3 (UNILAB) powder was impregnated with the desired amount of aqueous solutions of $Mg(NO_3)_2 \cdot 6H_2O$ xH_2O (98%, Acros Organics) and $ZrO(NO_3)_2 \cdot xH_2O$ (99.5%, Acros Organics). The wet powder was left at ambient temperature for 12 h. Thereafter, the samples were dried at 60 ºC for 24 h and calcined at 600 ºC for 4 h. Then, samples were pelletized and collected at the size range of 355 µm to 710 µm.

2.2 *Characterization methods*

A specific surface area, total pore volume, and average pore size diameter were calculated by Brunauer-Emmett-Teller (BET) model based on N_2 adsorption-desorption isotherm at –196 ºC measuring with Quantachrome Autosorb-iQ-MP. The sample was degassed at 100 ºC for 1 h and then at 300 ºC for another 3 h until vacuum pressure was lower than 10^{-2} kPa before the measurement.

X-ray powder diffraction (XRD) pattern was collected via Rigaku SmartLab® with Cu-Kα radiation at a scanning rate of 2°/min over the 2θ range of 2°–85°.

The morphology of the sample surface was investigated by scanning electron microscope (SEM) via FEI ESEM Quanta 450 FEG) and the elemental composition of materials were identified by energy dispersive X-ray analysis (EDX).

Temperature programmed desorption of O_2 (O_2-TPD) studies were performed employing BELCAT BASIC® for the measurement of the oxygen mobility of samples. Prior to the measurement, helium at a flow rate of 30 mL/min was supplied for 1 h to the reactor at 200 °C to remove any contaminants from the surface of the sample. Then, the adsorption of O_2 was processed at 200 °C for 1 h. Afterward, helium at 30 mL/min was supplied to the reactor again in order to purge out any O_2 residue and to cool down the sample to 40 ºC. The O_2 desorption was investigated in helium flow from 40 ºC to 900 ºC at a heating rate of 10 ºC/min and the adsorbed O_2 was detected by a thermal conductivity detector (TCD).

Temperature programmed desorption of CO_2 (CO_2-TPD) studies were performed for the measurement of the basicity of samples (BELCAT BASIC®). To prepare the sample surface, the sample was heated at 200 ºC for 1 h in helium flow to remove contaminants. The adsorption of CO_2 was operated at 40 ºC with a CO_2 flow at 30 mL/min for 1 h, followed by a helium purge for 20 min to remove the physisorbed CO_2. The CO_2 desorption was investigated from 40 ºC to 900 ºC at a heating rate of 10 ºC/min. The adsorbed CO_2 was monitored by TCD.

Operation of some characterization items can refer to the literature [26]–[31].

3 Results and Discussion

3.1 *BET analysis*

The specific surface area (S_{BET}), total pore volume (V_{Total}), and average pore size (D_{pore}) of all samples are given in Table 1. As observed in Table 1, Al_2O_3 presented S_{BET} of 95 m^2/g, V_{Total} of 0.25 cm^3/g, and D_{pore} of 6.3 nm. From the results, the addition of MgO and ZrO_2 onto Al_2O_3 (10M/A, 5M5Z/A, and 10Z/Al) caused a decrease in S_{BET} and V_{Total}. It is indicated that the Al_2O_3 surface is covered by MgO and ZrO_2.

Considering the result of 10M/A, the addition of 10 wt% MgO displayed the smaller S_{BET} (92 m^2/g) with the lower V_{Total} (0.20 cm^3/g) and a smaller D_{pore} (3.2 nm) than Al_2O_3. Meanwhile, 10Z/A showed the lowest S_{BET} (88m^2/g), V_{Total} of 0.23 cm^3/g, and the largest average pore size (8.1 nm). The sample of 5M5Z/A represented the textural properties between 10M/A and 10Z/A (S_{BET} of 90 m^2/g, V_{Total} of 0.22 cm^3/g, and D_{pore} of 7.4 nm). The different textural properties of the impregnated samples are ascribed to the particle size of metal oxide being added. As can be seen in the results, Al_2O_3 doped ZrO_2 shows a higher effect of pore blocking than Al_2O_3 doped MgO [32], [33]. It indicated that the ZrO_2 particles should be larger than MgO particles. The 5M5Z/A exhibited

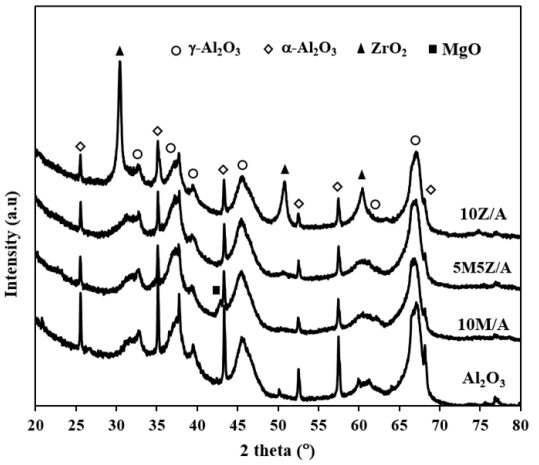

Figure 1: XRD patterns of Al_2O_3, 10M/A, 5M5Z/A, and 10Z/A.

a larger S_{BET} with a smaller D_{pore} than 10Z/A. This result means that mixing MgO with ZrO_2 can against the migration of ZrO_2 resulting in the decrease of pore blocking effect of the ZrO_2.

Table 1: BET analysis of MgO and ZrO_2 on Al_2O_3

Sample	S_{BET} (m^2/g)	V_{Total} (cm^3/g)	D_{pore} (nm)
Al_2O_3	95	0.25	6.3
10M/A	92	0.20	3.2
5M5Z/A	90	0.22	7.4
10Z/A	88	0.23	8.1

3.2 *XRD analysis*

The phase and crystalline structure of all samples were characterized via XRD analysis and diffractograms are illustrated in Figure 1. The diffractogram of Al_2O_3 represents the pattern of the mixed crystalline between α-Al_2O_3 (at 2θ = 25°, 35°, 44°, 52°, 58° and 68°) and γ-Al_2O_3 (at 2θ = 33° 36.5°, 39°, 46°, 61° and 67°). It can be observed that the peak intensity of Al_2O_3 was decreased when MgO was added to the surface (10M/A). However, a small diffraction peak of MgO appeared at 2θ of 43° indicating the dispersion of MgO on the Al_2O_3 surface or MgO possibly merged with Al_2O_3 to form the spinel structure (Al_2MgO_4) [34].

Meanwhile, the characteristic peaks at 2θ of 30°, 50°, and 60° of tetragonal ZrO_2 (t-ZrO_2) were observed only in 10Z/A [35]. Nonetheless, the diffraction peaks of MgO and ZrO_2 were not distinguished from the sample that involve both MgO and ZrO_2 (5M5Z/A). It can be implied that MgO may contribute to well dispersion of ZrO_2 on the Al_2O_3 surface. Moreover, the MgO diffraction peaks were rarely identified due to the sensitivity of this material and the below detectable limit of the MgO particle sizes [36].

3.3 *SEM-EDX analysis*

The surface morphology of Al_2O_3, 10M/A, 5M5Z/A, and 10Z/Al all samples are displayed as SEM images in Figure 2(a)–(d) respectively. According to the SEM images, the pore structure of the Al_2O_3 surface tends to be reduced after impregnating metal oxides. It can be explained by the pore blocking effect of the additional metal oxide.

Figure 3 presents EDX analysis of all modified Al_2O_3 samples. The data generated by EDX analysis consist of spectra showing peaks corresponding to the elements in the composition of the sample being analyzed. The contents of Al, Mg and Zr for each sample are revealed and reported in Table 2. The presence of Mg and Zr elements was confirmed by the EDX analysis and this result demonstrated a dispersion of MgO and ZrO_2 on the Al_2O_3 surface. It was observed that the percent composition of Al, Mg, and Zr are close to the desirability.

Table 2: EDX analysis of weight percent of Al, Mg, and Zr elements for 10M/A, 5M5Z/A, and 10Z/A

Sample	Weight Percentage (wt%) of Metal		
	Al	Mg	Zr
10M/A	89.3	10.7	-
5M5Z/A	87.8	6.2	6.0
10Z/A	89.9	-	10.1

3.4 *O_2-TPD*

The oxygen mobility of the adsorbent was investigated using temperature-programmed desorption of O_2 (O_2-TPD) measurement. The O_2 desorption reflects the mobile oxygen species on the solid sorbent surface. O_2-TPD profiles (Figure 4) could be deconvoluted into peaks of three temperature ranges. Peaks in the range of 50 ºC to 200 ºC are the adsorbed oxygen species at the surface. Peaks that appeared at 200 ºC to 500 ºC are ascribed to the adsorbed oxygen species underneath the surface. Peaks at a temperature higher

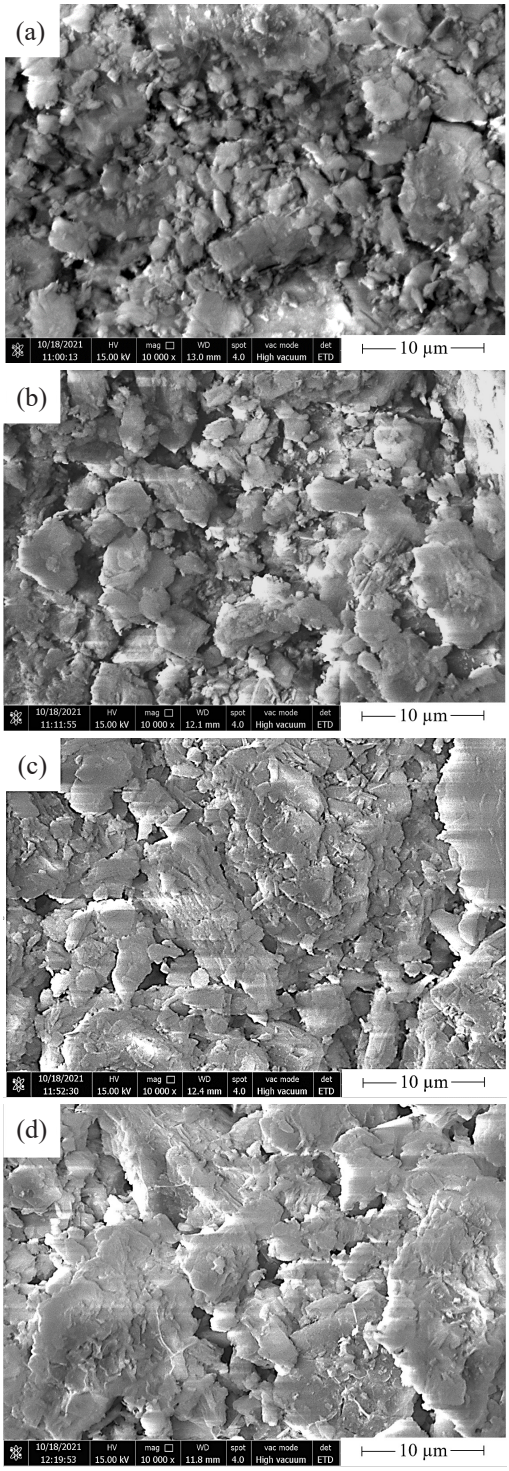

Figure 2: SEM images of (a) Al_2O_3, (b) 10M/A, (c) 5M5Z/A, and (d) 10Z/A.

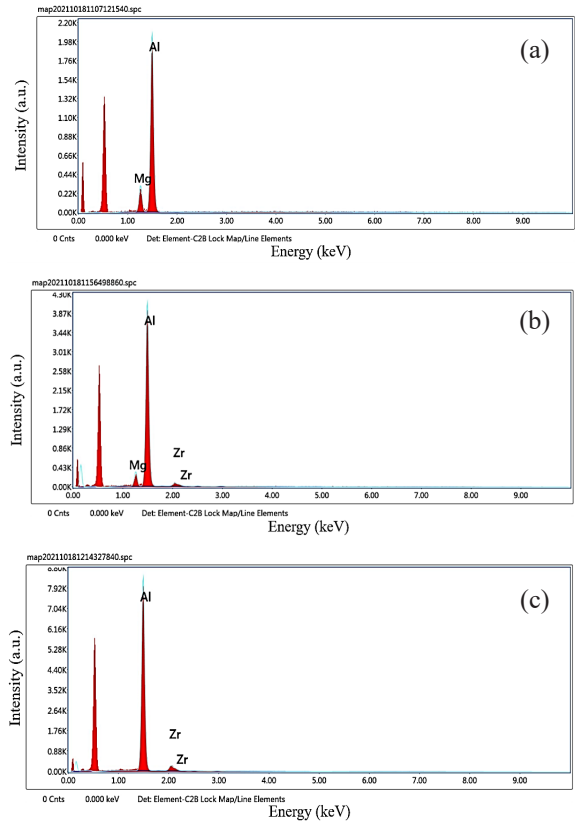

Figure 3: EDX analysis of (a)10M/A, (b) 5M5Z/A, and (c) 10Z/A.

than 500 ºC correlate to the desorption of bulk lattice oxygen [37]–[39].

The amount of oxygen mobility of Al_2O_3, 10M/A, 5M5Z/A, and 10Z/A are reported in Table 3. The oxygen mobility of Al_2O_3 was 1.847 mmol/g. From the results, modified Al_2O_3 samples (10M/A, 5M5Z/A, and 10Z/A) provided higher oxygen mobility than Al_2O_3. 10M/A and 10Z/A gave the total oxygen vacancies at 1.970 and 2.883 mmol/g, respectively. For 5M5Z/A, the oxygen mobility increased to 3.136 mmol/g. Thus, the mixed MgO-ZrO_2 can greatly enhance the oxygen mobility of Al_2O_3. Al_2O_3 involving ZrO_2 on the surface provided high oxygen mobility because ZrO_2 is the oxygen vacancy material. Al_2O_3 with Mg-Zr mixed oxide on the surface showed the highest oxygen vacancy sites because Mg^{2+} from MgO has an ionic radius of 0.65 Å which is smaller than Zr^{4+} (0.79 Å). Therefore, Mg^{2+} can substitute into ZrO_2 lattice resulting in more oxygen vacancy creation [36].

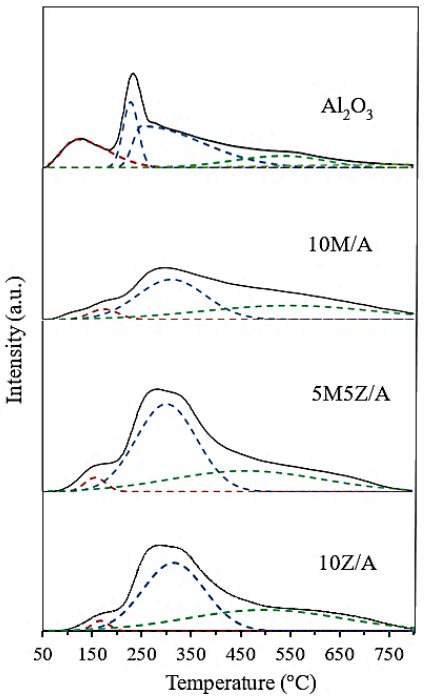

Figure 4: O_2-TPD profiles of Al_2O_3, 10M/A, 5M5Z/A, and 10Z/A.

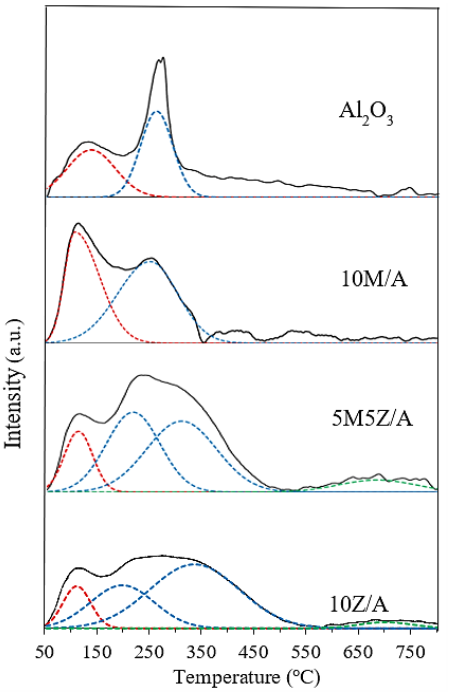

Figure 5: CO_2-TPD profile of Al_2O_3,10M/A, 5M5Z/A, and 10Z/A.

Table 3: O_2-TPD profile of Al_2O_3,10M/A, 5M5Z/A, and 10Z/A

Sample	Oxygen Mobility (mmol/g)			
	50–200 ºC	200–500 ºC	> 500 ºC	Total Oxygen Vacancy Site
Al_2O_3	0.656	0.869	0.322	1.847
10M/A	0.202	0.915	0.853	1.970
5M5Z/A	0.222	2.150	0.763	3.136
10Z/A	0.271	1.882	0.730	2.883

3.5 *CO_2-TPD*

The CO_2-TPD technique begins with the adsorption isotherm of CO_2 on the clean surface of the material. Then, flushing the physisorbed CO_2 by the inert gas. Afterward, the temperature increased at the constant heating rate that the chemisorbed CO_2 was desorbed from different basic site strengths (Figure 5). Moreover, the total CO_2 desorption represents the total number of basic sites as well as the CO_2 adsorption capacity. Figure 5 shows the CO_2-TPD profiles of Al_2O_3, 10M/A, 5M5Z/A, and 10Z/A. Desorbed CO_2 could be attributed to adsorbed CO_2 on basic sites of materials. The distribution of basic site strength was determined using the area under the curve fitted by Gaussian calculation. CO_2 desorption peaks of all profiles could be evaluated into three temperature ranges of 50–200 ºC, 200–500 ºC, and 500–900 ºC that are assigned to the desorption of weak, moderate, and strong adsorbed CO_2, respectively due to the types of basic sites on the adsorbent surface. The weak basic sites correspond to Brønsted hydroxyl groups, moderate basic sites are associated with the Lewis acid-base pairing, and strong basic sites are attributed to low-coordination surface oxygen (O^{2-}) anions. The CO_2 adsorbed species are summarized in Table 4 accompanied by their structure [40]–[42].

The amount of each basic site was analyzed based on the peak area and the total amount of basic sites exhibit the CO_2 adsorption capacities concluding in Table 5. The CO_2 adsorption capacities are shown as a bar chart in Figure 6. As seen in Table 5, the adsorption of CO_2 on Al_2O_3 was detected only in weak and moderate basic sites, which is the property of the commercial Al_2O_3. Among all samples, Al_2O_3 has the lowest adsorption capacity of CO_2 (0.873 mmol/g).

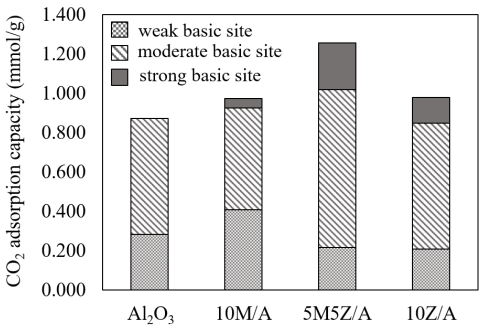

Figure 6: CO_2 adsorption capacity of Al_2O_3,10M/A, 5M5Z/A, and 10Z/A.

Table 4: Adsorbed CO_2 species on the surface of solid sorbent

Basic Site Strength	Adsorbed Species	Adsorption Site
Weak	Bicarbonate	Hydroxyl groups, Brønsted
Moderate	Bidentate Carbonate	Acid-base pairing, Lewis
Strong	Monodentate Carbonate	Low-coordination O^{2-}, Lewis

Table 5: CO_2-TPD profile of Al_2O_3,10M/A, 5M5Z/A, and 10Z/A

Sample	Basic Sites (mmol/g)			
	Weak	Moderate	Strong	Total/ CO_2ads.cap.
Al_2O_3	0.284	0.589	-	0.873
10M/A	0.409	0.517	0.047	0.973
5M5Z/A	0.217	0.801	0.236	1.254
10Z/A	0.208	0.640	0.131	0.979

Comparisons in Table 5 and Figure 6 represents that the addition of MgO and/or ZrO_2 onto Al_2O_3 improved the CO_2 adsorption capacity of Al_2O_3. For the addition of MgO (10M/A), the amount of weak and strong basic sites increased. The CO_2 adsorption capacity is more informative to consider the CO_2 adsorption performance. The CO_2 adsorption capacity of 10M/A is 0.973 mmol/g which increased about 11% from the CO_2 capacity of Al_2O_3. This result suggests the appearance of more basic sites that are ascribed to MgO. The additional ZrO_2 (10Z/A) increased the amount of moderate significantly. Then, the CO_2 adsorption capacity of 10Z/A increased to 0.979 mmol/g. Impregnating mixed metal oxides of MgO-ZrO_2 onto the Al_2O_3 (5M5Z/A) greatly enhanced the amount of moderate and strong basic sites and gave the highest CO_2 adsorption capacity. The CO_2 adsorption capacity of this sample was 1.254 mmol/g that increased 1.4 times higher than that of pure Al_2O_3.

The trend of oxygen mobility is similar to the trend of CO_2 adsorption capacity of all samples. It suggests that the oxygen mobility occurred by additional oxygen vacancy material plays an important role in CO_2 adsorption. Xin *et al.* reported that the oxygen vacancy acts as Lewis basic site and CO_2 is a Lewis acid [43]. This site can migrate consequence of the oxygen vacant position. CO_2 molecules are adsorbed on this site by filling the oxygen atom in the missing oxygen position causing in carbonate species at the surface [44]–[46]. These species will then become bidentate carbonate larger than monodentate carbonate [47]. Therefore, ZrO_2 incorporated with MgO prevents the migration of ZrO_2 and creates more oxygen vacancy sites. As a result, Mg-Zr mixed oxide modified Al_2O_3 produces a large amount of CO_2 adsorption sites that show a relatively high CO_2 adsorption capacity.

4 Conclusions

This study revealed the potential of Mg-Zr mixed oxide (MgO-ZrO_2) as a co-functional material to modify the Al_2O_3 surface for CO_2 adsorption. Compared to Al_2O_3, the impregnation of MgO, ZrO_2, or MgO-ZrO_2 onto Al_2O_3 enhanced the oxygen mobility and basicity of the Al_2O_3 surface, which increases the CO_2 adsorption. Among all samples, MgO-ZrO_2 modified Al_2O_3 provided the highest oxygen mobility of 3.136 mmol/g and showed the greatest CO_2 adsorption capacity of 1.254 mmol/g. It is because ZrO_2 incorporated with MgO create more oxygen vacancy sites than ZrO_2. This vacant site can be filled by oxygen atom of a CO_2 molecule, which forms carbonate species at the surface and splits into bidentate or monodentate carbonates. Consequently, the Mg-Zr mixed oxide increases the number of basic sites for moderate and strong basic strength on the Al_2O_3 surface. Thus, Mg-Zr mixed oxide modified Al_2O_3 is a great adsorbent of CO_2 and can be used as a support of catalysts for CO_2 utilization.

Acknowledgments

The authors gratefully acknowledge the research grant

from the Faculty of Applied Science, King Mongkut's University of Technology North Bangkok (grant number. 653119).

Author Contributions

T.C.: research design, methodology, investigation, data analysis, writing an original draft; S.J.: conceptualization, research design, methodology, investigation, data analysis, writing an original draft reviewing, and editing; T.R.: methodology, and data analysis; S.T.: data analysis and editing; M.P.: conceptualization, data curation, writing-reviewing and editing, funding acquisition project administration. All authors have read and agreed to the published this version of the manuscript.

Conflicts of Interest

The authors declare no conflict of interest.

References

[1] K. Adler, "Global CO_2 emissions to rise by 4.9% in 2021," 2021. [Online]. Available: https://cleanenergynews.ihsmarkit.com

[2] R. Lindsey, "Climate change: Atmospheric carbon dioxide," 2020 [Online]. Available: https://www.climate.gov

[3] D. I. Ferrer, *Supported Layered Double Hydroxides as CO_2 Adsorbents for Sorption-Enhanced H_2 Production*. Switzerland: Springer International Publishing, May. 2016.

[4] B. Acar, M. S. Başar, B. M. Eropak, B. S. Caglayan, and A. E. Aksoylu, "CO_2 adsorption over modified AC samples: A new methodology for determining selectivity," *Catalysis Today*, vol. 301, pp. 112–124, Mar. 2018.

[5] L. Li, N. Zhao, W. Wei, and Y. Sun, "A review of research progress on CO_2 capture, storage, and utilization in Chinese Academy of Sciences," *Fuel*, vol. 108, pp. 112–130, Jun. 2013.

[6] F. Wang, C. Gunathilake, and M. Jaroniec, "Development of mesoporous magnesium oxide-alumina composites for CO_2 capture," *Journal of CO_2 Utilization*, vol. 13, pp. 114–118, Mar. 2016.

[7] B. Acar, M. S. Başar, B. M. Eropak, B. S. Caglayan, and A. E. Aksoylu, "CO_2 adsorption over modified AC samples: A new methodology for determining selectivity," *Catalysis Today*, vol. 301, pp. 112–124, Mar. 2018.

[8] E. Takaluoma, T. Pikkarainen, and K. Kemppainen, "Adsorption and desorption of metals onto reusable adsorbent," 2018. [Online]. Available: http://www.mwen.info

[9] X. Jiao, L. Li, H. Li, F. Xiao, N. Zhao, W. Wei, and B. Zhang, "Influence of preparation parameters on the structural properties and the CO_2 capture performance of Mg–Zr solid sorbent," *Materials Research Bulletin*, vol. 64, pp. 163–170, Apr. 2015.

[10] P. Tobarameekul, S. Sangsuradet, N. N. Chat, and P. Worathanakul, "Enhancement of CO_2 adsorption containing zinc-ion-exchanged zeolite NaA synthesized from rice husk ash," *Applied Science and Engineering Progress*, vol. 15, no. 1, Nov. 2022, Art. no. 3640, doi: 10.14416/j.asep.2020.11.006.

[11] J. Foungchuen, N. Pairin, and C. Phalakornkule, "Impregnation of chitosan onto activated carbon for adsorption selectivity towards CO_2: Biohydrogen purification," *KMUTNB: International Journal of Applied Science and Technology*, vol. 9, no. 3, pp. 197–209, Apr. 2016, doi: 10.14416/j.ijast.2016.03.003.

[12] F. Chen, "Aluminum coordination and Lewis acidity in transition aluminas," *Journal of Catalysis*, vol. 133, no. 2, pp. 263–278, 1992.

[13] X. Jiao, L. Li, N. Zhao, F. Xiao, and W. Wei, "Synthesis and low-temperature CO_2 capture properties of a novel Mg–Zr solid sorbent," *Energy & Fuels*, vol. 27, no. 9, pp. 5407–5415, Jul. 2013.

[14] M. Haneda, K. Takamura, Y. Doi, N. Bion, and L. Vivier, "Synthesis of ordered porous zirconia containing sulfate ions and evaluation of its surface acidic properties," *Journal of Materials Science*, vol. 52, no. 10, pp. 5835–5845, May 2017.

[15] X. Wang, J. Zhao, Y. Li, S. Huang, J. An, R. Shi, and J. Ren, "Effects of surface acid–base properties of ZrO_2 on the direct synthesis of DMC from CO_2 and methanol: A combined DFT and experimental study," *Chemical Engineering Science*, vol. 229, Jan. 2021, Art. no. 116018.

[16] W. Sumarasingha, S. Supasitmongkol, and

M. Phongaksorn, "The effect of ZrO_2 as different components of Ni-Based catalysts for CO_2 reforming of methane and combined steam and CO_2 reforming of methane on catalytic performance with coke formation," *Catalysts*, vol. 11, no. 8, Aug. 2021, Art. no. 984.

[17] X. Liu, J. Ding, X. Lin, R. Gao, Z. Li, and W.-L. Dai, "Zr-doped CeO_2 nanorods as versatile catalyst in the epoxidation of styrene with tert-butyl hydroperoxide as the oxidant," *Applied Catalysis A: General*, vol. 503, pp. 117–123, Aug. 2015.

[18] R. V. Siriwardane, C. Robinson, M. Shen, and T. Simonyi, "Novel regenerable sodium-based sorbents for CO_2 capture at warm gas temperatures," *Energy and Fuels*, vol. 21, no. 4, pp. 2088–2097, Jul. 2007.

[19] H. Hayashi, J. Taniuchi, N. Furuyashiki, S. Sugiyama, S. Hirano, N. Shigemoto, and T. Nonaka, "Efficient recovery of carbon dioxide from flue gases of coal-fired power plants by cyclic fixed-bed operations over K_2CO_3-on-Carbon," *Industrial & Engineering Chemistry Research*, vol. 37, no. 1, pp. 185–191, Jan. 1998

[20] L. Li, X. Wen, X. Fu, F. Wang, N. Zhao, F. Xiao, W. Wei, and Y. Sun, "MgO/Al_2O_3 sorbent for CO_2 capture," *Energy & Fuels*, vol. 24, no. 10, pp. 5773–5780, Oct. 2010.

[21] A. Zukal, J. Pastva, and J. Čejka, "MgO-modified mesoporous silicas impregnated by potassium carbonate for carbon dioxide adsorption," *Microporous and Mesoporous Materials*, vol. 167, pp. 44–50, Feb. 2013.

[22] V. Hornebecq, C. Knöfel, P. Boulet, B. Kuchta, and P. L. Llewellyn, "Adsorption of carbon dioxide on mesoporous zirconia: Microcalorimetric measurements, adsorption isotherm modeling, and density functional theory calculations," *The Journal of Physical Chemistry C*, vol. 115, no. 20, pp. 10097–10103, May. 2011.

[23] K. Piyapaka, S. Tungkamani, and M. Phongaksorn, "Effect of strong metal support interactions of supported Ni and Ni-Co catalyst on metal dispersion and catalytic activity toward dry methane reforming reaction," *KMUTNB: International Journal of Applied Science and Technology*, vol. 9, no. 4, pp. 255–259, Oct. 2016, doi: 10.14416/j.ijast.2016.10.001.

[24] G. Chavez-Esquivel, J. C. Garcia-Martinez, J. A. De Los Reyes, V. A. Suárez-Toriello, M. A. Vera-Ramirez, and L. Huerta, "The influence of Al_2O_3 content on Al_2O_3-ZrO_2 composite-textural structural and morphological studies," *Materials Research Express*, vol. 6, no. 10, Aug. 2019, Art. no. 105201.

[25] T. Yan, W. Bing, M. Xu, Y. Li, Y. Yang, G.Cui, and M.Wei, "Acid–base sites synergistic catalysis over Mg–Zr–Al mixed metal oxide toward synthesis of diethyl carbonate," *RSC Advances*, vol. 8, no. 9, pp. 4695–4702, Aug. 2018.

[26] B. Zen, Z. Pan, L. Shen, D. Zhao, J. Teng, H. Hong, and H. Lin, "Effects of polysaccharides' molecular structure on membrane fouling and the related mechanisms," *SSRN Electronic Journal*, vol. 836, Aug. 2022, Art. no. 155579.

[27] B. Chen, X. Hu, J. Wang, R. Li, L. Shen, Y. Xu, and H. Lin, "Novel catalytic self-cleaning membrane with peroxymonosulfate activation for dual-function wastewater purification: Performance and mechanism," *Journal of Cleaner Production*, vol. 355, Jun. 2022, Art. no. 131858.

[28] J. Liu, L. Shen, H. Lin, Z. Huang, H. Hong, and C. Chen, "Preparation of Ni@UiO-66 incorporated polyethersulfone (PES) membrane by magnetic field assisted strategy to improve permeability and photocatalytic self-cleaning ability," *Journal of Colloid and Interface Science*, vol. 618, pp. 483–495, Jul. 2022.

[29] Z. Pan, B. Zeng, H. Lin, J. Teng, H. Zhang, H. Hong, and M. Zhang, "Fundamental thermodynamic mechanisms of membrane fouling caused by transparent exopolymer particles (TEP) in water treatment," *SSRN Electronic Journal*, vol. 802, no. 10, May 2021, Art. no.153252.

[30] R. Zhang, Y. Xu, L. Shen, R. Li, and H. Lin, "Preparation of Nickel@Polyvinyl alcohol (PVA) conductive membranes to couple a novel electrocoagulation-membrane separation system for efficient oil-water separation," *SSRN Electronic Journal*, vol. 653, Jul. 2022, Art. no. 120541.

[31] L. Han, C. Chen, L. Shen, H. Lin, B. Li, Z. Huang, and H. Hong, "Novel membranes with extremely high permeability fabricated by 3D printing and nickel coating for oil/water separation," *Journal of Materials Chemistry A*, vol. 10, no. 22, pp. 12055–12061, May. 2022.

[32] S. Gandhi and S. Patel, "Dry reforming of methane over supported nickel catalysts promoted by zerconia, ceria and magnesia," *International Journal of Advanced Research in Engineering and Technology (IJARET)*, vol. 6, no. 10, pp. 131–146, Oct. 2015.

[33] Zh. Li, Ch. Liu, X. Zhang, W. Wang, B. Wang, and X. Ma, "Effect of ZrO_2 on catalyst structure and catalytic sulfur-resistant methanation performance of $MoO_3/ZrO_2–Al_2O_3$ catalysts," *Kinetics and Catalysis*, vol. 59, no. 4, pp. 481–488, Aug. 2018.

[34] N. I. Radishevskaya, Y. A. Nazarova, O. V. Lvov, N. G. Kasatsky, and V. D. Kitler, "Synthesis of magnesium aluminate spinel in the $MgO-Al_2O_3$-Al system using the SHS method," *Journal of Physics: Conference Series*, vol. 1214, Apr. 2019, Art. no. 012019.

[35] M. S. Lanre, A. S. Al-Fatesh, A. H. Fakeeha, S. O. Kasim, A. A. Ibrahim, A. S. Al-Awadi, and A. E. Abasaeed, "Catalytic performance of lanthanum promoted Ni/ZrO_2 for carbon dioxide reforming of methane," *Processes*, vol. 8, no. 11, Nov. 2020, Art. no. 1502.

[36] X. Jiao, L. Li, N. Zhao, F. Xiao, and W. Wei, "Synthesis and low-temperature CO_2 capture properties of a novel Mg-Zr solid sorbent," *Energy & Fuels*, vol. 27, no. 9, pp. 5407–5415, Aug. 2013.

[37] Z. Qu, Z. Wang, X. Zhang, and H. Wang, "Role of different coordinated Cu and reactive oxygen species on the highly active Cu–CE–ZR mixed oxides in NH_3-SCO: A combined in situ EPR and O_2-TPD approach," *Catalysis Science & Technology*, vol. 6, no. 12, pp. 4491–4502, Feb. 2016.

[38] W. Liu, L. Li, X. Zhang, Z. Wang, X. Wang, and H. Peng, "Design of Ni-ZrO_2@SiO_2 catalyst with ultra-high sintering and coking resistance for dry reforming of methane to prepare syngas," *Journal of CO_2 Utilization*, vol. 27, pp. 297–307, Oct. 2018.

[39] E. I. Kauppi, K. Honkala, A. O. I. Krause, J. M. Kanervo, and L. Lefferts, "ZrO_2 Acting as a redox catalyst," *Topics in Catalysis*, vol. 59, no. 8–9, pp. 823–832, Apr. 2016

[40] N. Dharmasaroja, T. Ratana, S. Tungkamani, T. Sornchamni, D. S. A. Simakov, and M. Phongaksorn, "CO_2 reforming of methane over the growth of hierarchical Ni nanosheets/Al_2O_3-MgO synthesized via the ammonia vapour diffusion impregnation," *The Canadian Journal of Chemical Engineering*, vol. 99, no. S1, pp. S585–S595, Oct. 2021

[41] A. Smalenskaite, M. M. Kaba, I. Grigoraviciute-Puroniene, L. Mikoliunaite, A. Zarkov, R. Ramanauskas, and A. Kareiva, "Sol–gel synthesis and characterization of coatings of Mg-Al layered double hydroxides," *Materials*, vol. 12, no. 22, Nov. 2019, Art. no. 3738.

[42] L. Santamaria, A. Arregi, J. Alvarez, M. Artetxe, M. Amutio, G. Lopez, and M. Olazar, "Performance of a Ni/ZrO_2 catalyst in the steam reforming of the volatiles derived from biomass pyrolysis," *Journal of Analytical and Applied Pyrolysis*, vol. 136, pp. 222–231, Nov. 2018.

[43] C. Xin, M. Hu, K. Wang, and X. Wang, "Significant enhancement of photocatalytic reduction of CO_2 with H_2O over ZnO by the formation of basic zinc carbonate," *Langmuir*, vol. 33, no. 27, pp. 6667–6676, Jun. 2017.

[44] B. Liu, C. Li, G. Zhang, X. Yao, S. S. C. Chuang, and Z. Li, "Oxygen vacancy promoting dimethyl carbonate synthesis from CO_2 and methanol over Zr-doped CeO_2 nanorods," *ACS Catalysis*, vol. 8, no. 11, pp. 10446–10456, Oct. 2018.

[45] S. Song, J. Wei, X. He, G. Yan, M. Jiao, W. Zeng, and M. Shi, "Oxygen vacancies generated by Sn-doped ZrO_2 promoting the synthesis of dimethyl carbonate from methanol and CO_2," *RSC Advances*, vol. 11, no. 56, pp. 35361–35374, Nov. 2021.

[46] X. Wan, L.Wang, S.Gao, X. Lang, L. Wang, T. Zhang, and W. Wang, "Low-temperature removal of aromatics pollutants via surface labile oxygen over Mn-based mullite catalyst $SmMn_2O_5$," *Chemical Engineering Journal*, vol. 410, Apr. 2021, Art. no. 128305.

[47] Y. Wang, A. Lafosse, and K. Jacobi, "Adsorption and reaction of CO_2 on the RuO_2(110) surface," *Surface Science*, vol. 481, no. 1–3, pp. 113–118, Jun. 2001.